PHYSICAL REVIEW B VOLUME 55, NUMBER 21 1 JUNE 1997-I

Coherent magnetic structures in terbium/holmium superlattices

C. Bryn-Jacobsen and R. A. Cowley
Oxford Physics, Clarendon Laboratory, Parks Road, Oxford, OX1 3PU, United Kingdom

D. F. McMorrow
Department of Solid State Physics, Risø National Laboratory, DK-4000 Roskilde, Denmark

J. P. Goff, R. C. C. Ward, and M. R. Wells
Oxford Physics, Clarendon Laboratory, Parks Road, Oxford, OX1 3PU, United Kingdom

(Received 23 December 1996)

Neutron-scattering techniques have been used to investigate the magnetic properties of three Tb/Ho superlattices grown by molecular-beam epitaxy. It is revealed that for temperatures in the range $T=10$ to $T_N(\mathrm{Ho})\approx 130$ K, there is a basal-plane ferromagnetic alignment of Tb moments within Tb blocks that is coherent with a basal-plane helical ordering of Ho moments. Between $T\approx T_N(\mathrm{Ho})$ and 200 K, the Tb moments remain ferromagnetically aligned within Tb blocks, with adjacent Tb blocks antiferromagnetically coupled. As the temperature is raised from $T\approx 200$ to 230 K, two samples retain this magnetic structure while the third undergoes a transition first to a mixed phase of helically and ferromagnetically ordered Tb moments, then to a phase with only helically ordered Tb moments. In all cases, the magnetic ordering is found to be long ranged, with coherence lengths extending over three to six bilayers. The results are discussed with a consideration of previous rare-earth superlattice studies, and the possible mechanisms for interlayer coupling. [S0163-1829(97)01421-5]

I. INTRODUCTION

Early investigations of the magnetic properties of rare-earth superlattices concentrated on magnetic/nonmagnetic combinations. The long-range coherent ordering of elements such as Gd (Ref. 1) and Dy (Ref. 2) over nonmagnetic interlayers encouraged the development of models for the interlayer coupling mechanisms. These were originally based upon a conventional Ruderman-Kittel-Kasuya-Yosida (RKKY) interaction, in which the localized $4f$ moments in the magnetic blocks spin polarize the conduction electrons in adjacent nonmagnetic blocks. The peak in the conduction-electron susceptibility $\chi(\boldsymbol{q})$ for the nonmagnetic layers was considered to determine the form of the induced moments, with the spin-density wave in the nonmagnetic region mediating the coupling required for coherent magnetic ordering. It was suggested that this model was able to describe the magnetic properties of superlattices such as Gd/Y (Ref. 3) and Dy/Y.[3] For some superlattice combinations it has also been necessary to consider the influence of dipolar interactions. These interactions were reported to have been particularly important in Dy/Lu (Ref. 4) superlattices, and to affect the magnetic ordering in for example, Ho/Lu (Ref. 5) and Ho/Sc.[6]

The studies of rare-earth superlattices have since been extended to include magnetic/magnetic combinations. When both superlattice constituents are magnetically ordered, nearest-neighbor exchange interactions at the interfaces are an additional factor that may influence the magnetic ordering, and extensive modeling was used to illustrate their importance in some Gd/Dy (Ref. 7) samples. The results from these more complex systems have sustained an interest in the possible mechanisms for interlayer coupling. For example, an approach has been proposed recently that suggests in some cases long-range coherence is achieved by the establishment of a coherent band structure for the whole superlattice.[8,9] A primary necessary condition for the establishment of this overall band structure is believed to be the matching at the interfaces of the wave functions associated with the magnetic structures of the constituent elements. These ideas have been used to explain for instance, the lack of ordering of the c-axis components of Er moments over Ho blocks in Ho/Er,[8] and the suppression of the ferromagnetic phase of Dy in Dy/Ho (Ref. 9) superlattices.

Despite continuing activity in the field,[10] there are still relatively few reports on magnetic/magnetic rare-earth combinations. Here we present an investigation of the magnetic properties of Tb/Ho superlattices. The bulk structural characteristics of Tb and Ho are similar, with both elements adopting the hexagonal close-packed (hcp) crystal structure, with a mismatch in lattice parameters of less than 1.5%. However, the magnetic properties differ considerably both in the temperature range of the magnetic ordering, and in the details of the magnetic structures themselves. Two of the earliest reports of the magnetic properties of Tb are given by Koehler *et al.*,[11] and Dietrich and Als-Nielsen;[12] with a more recent study undertaken by Gehring *et al.*[13] It was found that at $T_N\approx 226$ K,[12] the Tb $4f^8$ moments align ferromagnetically in the basal plane, with an orientation that rotates between successive planes along the c axis. The wave vector $\boldsymbol{q}$ associated with this helical structure reduces on cooling from $\boldsymbol{q}=0.115\ \boldsymbol{c}^*$ at T_N to a minimum of $\boldsymbol{q}=0.091\ \boldsymbol{c}^*$ at $T_C\approx 216$ K. At this temperature, there is a first-order transition to a phase where the Tb moments are ferromagnetically aligned in the basal plane. However, Dietrich and Als-Nielsen[12] detected some helical ordering of Tb moments

down to $T \approx 212$ K. In this mixed phase region, the incommensurate wave vector increases as the temperature is decreased, with $\boldsymbol{q} \approx 0.105\ \boldsymbol{c}^*$ at $T \approx 212$ K. The properties of bulk Ho have also been extensively studied. Koehler *et al.*[14] showed that between $T_N \approx 132$ and 18 K, the Ho $4f^{10}$ moments align in a basal-plane helix. The wave vector reduces from $\boldsymbol{q} = 0.275\ \boldsymbol{c}^*$ at T_N to $\boldsymbol{q} = (1/6)\ \boldsymbol{c}^*$ at $T \approx 18$ K, below which the moments tilt out of the basal plane to form a ferromagnetic cone structure. The advent of x-ray magnetic scattering enabled Gibbs *et al.*[15] to establish that the wave vector locks in to a series of commensurable magnetic structures between $T \approx 30$ and 18 K. More recently neutron-scattering techniques have been used by Cowley and Bates,[16] and by Simpson *et al.*[17] to examine the low-temperature ordering in more detail.

There has been only one previous study of a rare-earth superlattice containing Tb, that of Tb/Y by Dufour *et al.*[18] They reported that the Tb moments aligned ferromagnetically in the basal plane below $T \approx 225$ K with the ordering largely confined to individual Tb blocks. Of the rare earths Dy (Ref. 19) possesses magnetic properties most similar to those of Tb, with a basal-plane helical ordering of moments between $T_N \approx 179$ K and $T_C \approx 87$ K, below which temperature the moments align ferromagnetically in the basal plane. Two possible examples of Dy-based superlattices that might be useful for comparison with Tb/Ho are Dy/Ho (Ref. 9) and Gd/Dy.[7,20,10] For Dy/Ho superlattices, Simpson *et al.*[9] found that between T_N(Dy) and T_N(Ho) the Dy moments ordered in a basal-plane helical structure with a long-range coherence length. Below T_N(Ho) both the Dy and the Ho moments ordered helically in the basal plane, with no evidence of the ferromagnetic structure of bulk Dy. For Gd/Dy (Refs. 7,20,10) superlattices, the details of the magnetic ordering were dependent upon the Dy block thickness. At $T \approx 290$ K, the Gd moments ordered ferromagnetically within Gd blocks, with adjacent Gd blocks antiferromagnetically aligned. Below $T \approx 180$ K, a helical ordering of Dy moments was also detected, and in most cases it was found that as the temperature was lowered the decrease in the Dy turn angle rotated adjacent Gd blocks towards a ferromagnetic alignment.

The procedures adopted for the growth of the Tb/Ho superlattices are outlined in Sec. II, while in Sec. III we detail the experimental techniques used for their investigation. In Sec. IV there is a description of the structural characterization of the samples and its use in the separation of the nuclear from magnetic scattering. Section V includes an explanation of the models used to identify and characterize the magnetic structures, together with the results from our analysis. These results are discussed in Sec. VI, with a consideration of previous superlattice studies and mechanisms for interlayer coupling.

II. SAMPLE GROWTH

Three Tb/Ho superlattices were grown by molecular-beam epitaxy (MBE) using a Balzers UMS 630 facility at the Clarendon Laboratory, Oxford. The growth techniques adopted were based upon those described by Jehan *et al.*,[21] and initially developed by Kwo *et al.*[22] Each sample was grown upon a sapphire substrate (with a surface area of approximately 1 cm^2), which had been pretreated by heating to a temperature of $T \approx 1000\,^\circ$C. 1500 Å of Nb was deposited upon the substrate to prevent chemical reaction with the rare earths. A 1800 Å Y-seed layer then followed to enable the lattice parameters to relax back to suitable values before the subsequent growth of the Tb and Ho superlattice layers. These superlattice layers were formed by depositing n_{Tb} layers of Tb followed by n_{Ho} layers of Ho at a rate of 0.5 Å s^{-1}, with this bilayer unit repeated 80 times. The Tb and Ho were evaporated from an electron-beam heated source and an effusion cell, respectively, with the calibration of the flux settings achieved using an *in situ* quartz-crystal monitor. During the rare-earth deposition the substrate temperature was held at 400 °C, which was considered to be sufficiently high to allow surface diffusion while still low enough to limit the extent of interfacial interdiffusion. The final structure was capped by 250 Å of Y to inhibit oxidation. The epitaxial relationships in the growth direction are $\{110\}Al_2O_3 \| \{110\}Nb \| \{001\}$Tb/Ho. The samples produced have nominal compositions Tb_{10}/Ho_{30}, Tb_{20}/Ho_{20}, and Tb_{30}/Ho_{10}, where the subscripts refer to the number of planes in a single bilayer.

III. EXPERIMENTAL PROCEDURES

The Tb/Ho superlattices were examined at the Clarendon Laboratory, Oxford, using a high-resolution triple-axis x-ray diffractometer mounted on a Stöe rotating anode generator operating at 6 kW. At $T = 290$ K, scans were performed with the wave-vector transfer $\boldsymbol{Q}$ along the $[00\ell]$ and $[10\ell]$ directions in reciprocal space, as well as transverse scans through the (002) nuclear Bragg peaks. The Tb_{20}/Ho_{20} sample was then placed in a closed-cycle cryostat, and using a lower resolution instrument additional scans were made with $\boldsymbol{Q}$ along $[00\ell]$ at $T = 10$ and 100 ± 3 K; and $T = 290 \pm 1$ K.

Neutron-scattering experiments were undertaken at Risø National Laboratory, Denmark, using the triple-axis spectrometer TAS1 situated on the cold source of the DR3 reactor. The samples were mounted with the $(h0\ell)$ plane in the scattering plane and positioned in a closed-cycle cryostat that enabled the sample temperature to be controlled to ± 0.5 K. Pyrolytic-graphite monochromator and analyzer crystals were set to select 5 meV neutrons, with a cooled beryllium filter employed to reduce higher-order contamination of the incident beam. Scans were performed with $\boldsymbol{Q}$ along the $[00\ell]$ and $[10\ell]$ directions at selected temperatures upon heating from $T = 10$ to 290 K. The reactor-to-sample collimations of $120' - 30' - 60' - 140'$ resulted in wave-vector resolutions in the scattering plane of 0.012 $Å^{-1}$ [full width at half maximum (FWHM)].

IV. STRUCTURAL ANALYSIS

Both x-ray- and neutron-scattering techniques were used to determine the structural properties of the samples. X-ray-scattering measurements of all the samples were performed at room temperature, and the results are summarized in Table I. The widths of the (002) peaks obtained from scans of $\boldsymbol{Q}$ along $[00\ell]$ can be used to deduce that the real-space coher-

TABLE I. The structural properties of the Tb/Ho superlattices deduced from x-ray measurements at $T=290$ K. The fitted compositions were calculated by fitting a model of the superlattice structure to scans of $\boldsymbol{Q}$ along [00ℓ] (Ref. 21). The d spacings are the separation of close-packed planes in the growth direction, and σ defines the width of interdiffusion at the interfaces (Ref. 21). The mosaic (spread) values are the FWHM of transverse scans through the (002) nuclear Bragg peaks, and give an indication of crystallographic quality. The coherence lengths (C. lengths) calculated from scans along [00ℓ] refer to the stacking of close-packed planes in the growth direction, while the lengths from scans along [10ℓ] give the coherence of the hcp stacking sequence.

Nominal $(n_{Tb}/n_{Ho})_N$	Fitted n_{Tb}/n_{Ho}	d_{Tb} ± 0.002 Å	d_{Ho} ± 0.002 Å	σ ± 1 plane	Mosaic $\pm 0.2°$	[00ℓ] C. length ± 150 Å	[10ℓ] C. length ± 250 Å
$(10/30)_{80}$	8.5/30.0	2.830	2.812	4.5	0.26	2600	1100
$(20/20)_{80}$	17.5/19.5	2.829	2.805	4.0	0.27	2500	1000
$(30/10)_{80}$	28.0/10.0	2.832	2.820	4.0	0.20	3400	1200

ence lengths ξ, of the stacking of close-packed planes in the growth direction since

$$\xi = 2\pi/\Delta\boldsymbol{Q}, \tag{1}$$

where $\Delta\boldsymbol{Q}$ is the FWHM in reciprocal space, and the very high resolution of the x-ray diffractometer can be neglected. Coherence lengths of approximately 2500 Å were found. Similarly, the width of the Bragg peaks observed when the wave-vector transfer was scanned along [10ℓ] indicate that the $ABAB\ldots$ hcp stacking sequence is coherent over at least 1000 Å. The FWHM of transverse scans through the main (002) peak provide a measure of the crystallographic perfection, here referred to as the mosaic spread of the samples. The values found of approximately 0.25° are comparable to those measured for other rare-earth superlattices grown by MBE,[21] and indicate that the samples are of good crystalline quality.

To obtain further quantitative information on the structural properties of the samples, the data obtained at $T=290$ K (well above the highest magnetic-ordering temperature) from the scans of $\boldsymbol{Q}$ along [00ℓ] using both x rays and neutrons were fitted independently to models of the superlattice structure described by Jehan *et al.*[21] Fits to the data for Tb_{30}/Ho_{10} are shown by the solid lines in Fig. 1. Using these models, values for n_{Tb}, n_{Ho}, d_{Tb}, and d_{Ho} were obtained (where the d spacings d_{Tb} and d_{Ho} are the separation of close-packed planes in the growth direction of Tb and Ho, respectively). The models include a simulation of interdiffusion at the interfaces using a tanh function, with a parameter σ defining the width of the interfaces. The values of σ obtained of approximately 4 ± 1 planes are typical for rare-earth superlattices.[21] All the structural parameters deduced by fitting independently models to the x-ray and neutron measurements agree within error, with the more accurate results obtained using x rays recorded in Table I. This structural characterization of the samples was then used to aid the analysis of the neutron-scattering results.

As outlined in Sec. I, the magnetic moments in bulk Tb align ferromagnetically in the basal plane for temperatures below $T\approx 220$ K, which results in magnetic scattering in the same region of reciprocal space as the nuclear scattering.[23] It will be shown in Sec. V that at most of the temperatures measured, a similar ferromagnetic ordering of Tb moments occurs in the Tb/Ho superlattices. One possible approach to study the magnetic scattering alone is to subtract the nuclear-scattering contribution from the total neutron scattering. This procedure was adopted for the scans along [00ℓ] and [10ℓ] by taking the nuclear-scattering contribution to be that measured at $T=290$ K, and this yielded satisfactory results for scans along [10ℓ]. However, it was found that for some scans along [00ℓ] at low temperatures, the subtraction results around (002) did not exhibit a smooth variation of intensity with wave vector, and there were a number of negative intensity values. These problems arise from a failure to account for the changes with temperature of the nuclear-scattering contribution due to the temperature dependence of the lattice parameters. These changes are more pronounced along [00ℓ] than [10ℓ], and additionally complicated along [00ℓ] due to the presence of the (002) Y peak [shown in Fig. 1(b)]. To ascertain the changes in position of the peaks due to the Tb/Ho layers, and the (002) Y peak, further x-ray measurements were taken for Tb_{20}/Ho_{20} at $T=10$, 100, and 290 K with $\boldsymbol{Q}$ scanned along [00ℓ]. Relative to their positions at $T=290$ K and to an accuracy of ± 0.002 Å^{-1}, there was a negligible change in the position with temperature of the main (002) Tb/Ho peak (at most 0.001 Å^{-1}), while the position of the (002) Y peak altered by up to 0.011 Å^{-1}. In

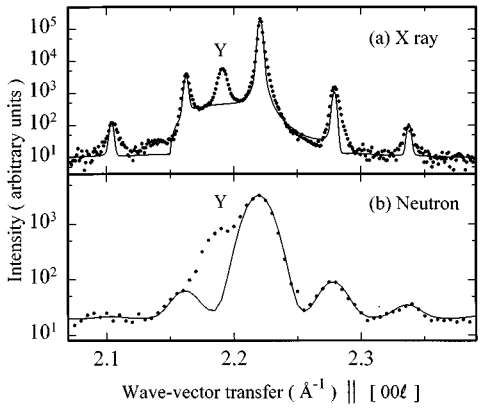

FIG. 1. The points show the nuclear scattering observed from Tb_{30}/Ho_{10} at $T=290$ K when scanning $\boldsymbol{Q}$ along [00ℓ] using (a) x rays, and (b) neutrons. The solid lines are fits to the data using the models described in Sec. IV. The peaks marked Y are due to scattering from the Y-seed and capping layers, and are not included in the models.

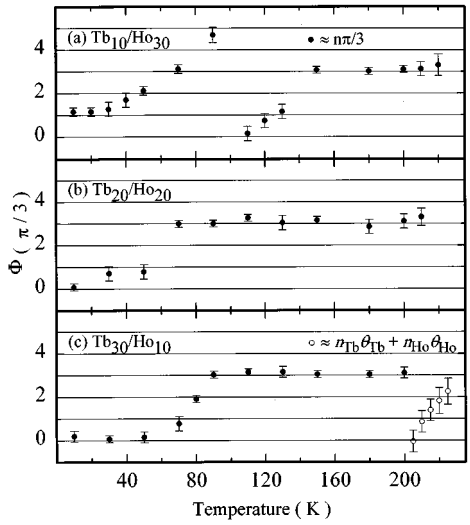

FIG. 2. The temperature variation of the total turn angle per bilayer Φ (modulo 2π) for (a) Tb_{10}/Ho_{30}, (b) Tb_{20}/Ho_{20}, and (c) Tb_{30}/Ho_{10}. The filled circles show the values calculated using the offset in the position of the magnetic peaks from the position of the (002) nuclear peaks. The open circles in (c) are the values of Φ (modulo 2π) for Tb_{30}/Ho_{10} calculated from fitted values of ϕ_{Tb} and ϕ_{Ho} above $T \approx 200$ K.

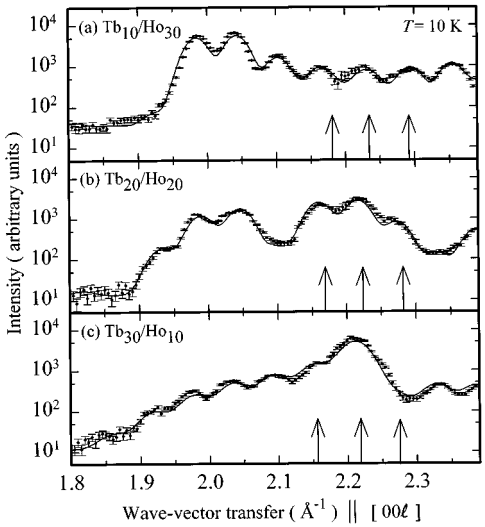

FIG. 3. The points show the magnetic-scattering results at $T = 10$ K from scans of $\boldsymbol{Q}$ along [00ℓ] using neutrons for the superlattices (a) Tb_{10}/Ho_{30}, (b) Tb_{20}/Ho_{20}, and (c) Tb_{30}/Ho_{10}. The solid lines are fits to the data using the model detailed in Sec. V, which simulates a basal-plane ferromagnetic ordering of Tb moments within Tb blocks, and a basal-plane helical ordering of Ho moments. The arrows indicate the positions of the main peaks in the fits of the model described in Sec. IV to the nuclear scattering at $T = 290$ K from the Tb/Ho layers.

order to isolate the contribution to the nuclear scattering due to the Y, the fits of models to the nuclear scattering from the Tb/Ho layers at $T = 290$ K [as illustrated for Tb_{30}/Ho_{10} in Fig. 1(b)] were subtracted from the total intensity to give the scattering from the Y for each sample, which could be fitted by a Gaussian. It was decided to construct the nuclear scattering along [00ℓ] at each temperature from the fits of models to the scattering from the Tb/Ho layers at $T = 290$ K, together with these Gaussian peaks, but with the characteristics of the Gaussian peaks suitably adjusted to account for the effects of changing temperature. To determine the appropriate adjustments, the more extensive data from neutron-scattering measurements of Nd/Pr (Ref. 24) superlattices was used for which the experimental details were the same as for the measurements of Tb/Ho. The Nd/Pr samples had Y-seed and capping layers of the same thicknesses as the Tb/Ho samples. However for Nd/Pr,[24] there was no magnetic ordering above $T \approx 30$ K, and when ordering occurred it did not influence the intensity of scattering in the region of the (002) Y peak. It was found that the amplitude and width of the Y peaks for all the Nd/Pr samples studied were to a good approximation independent of temperature. Therefore for each temperature measured, the position of the Gaussian Y peaks for the Tb/Ho superlattices were adjusted according to the position extracted from the Nd/Pr data, with the initial amplitudes and widths of the Gaussians held constant. A similar analysis was also made using the measurements from Ho/Pr (Ref. 25) superlattices (with Y-seed and capping layers), and the results were the same within error. The subtraction results displayed a smooth variation of intensity with wave vector, and no negative intensity values. The constructed magnetic scattering for scans along [00ℓ], together with the results for scans along [10ℓ] for which a straightforward subtraction was sufficient, could then be used to determine the magnetic properties of the samples.

V. MAGNETIC PROPERTIES

To identify and gain quantitative information on the magnetic ordering of the Tb/Ho superlattices, models of magnetic structures were fitted to the results from subtracting the nuclear scattering (which was constructed as described in Sec. IV) from the total neutron scattering. As outlined in Sec. I, the moments in bulk Tb align ferromagnetically in the basal plane below $T \approx 220$ K, whereas in bulk Ho a helical ordering is observed below $T \approx 132$ K with the moments confined to the basal plane above $T \approx 18$ K. In previous superlattice studies, the ordering of moments in the superlattice structures has often been similar to the bulk behavior of the constituent elements.[10] Therefore as a starting point, the basic model fitted to the data assumed that within basal planes of the Tb and Ho blocks, the moments were ordered ferromagnetically and helically, respectively. This model was based upon that detailed by Jehan *et al.*[21] for Ho/Y superlattices to describe the magnetic scattering observed when $\boldsymbol{Q}$ was scanned along [00ℓ], and also the extension by Simpson *et al.*[8] for $\boldsymbol{Q}$ scanned along [10ℓ]. Interdiffusion at the interfaces is included by use of a tanh function of the same form as that used for the modeling of the structural data.[21] The Tb/Ho model was then fitted to the magnetic scattering using a least-squares algorithm, with simultaneous fits for the results from scanning $\boldsymbol{Q}$ along [00ℓ] and [10ℓ] at each temperature measured.

The structural data analysis was used to give initial values for n_{Tb}, n_{Ho}, d_{Tb}, d_{Ho}, and σ. To obtain initial values for the turn angle per plane in the Ho layers ϕ_{Ho}, the temperature-dependent values for the total turn angle per bilayer Φ were first considered. As shown by Jehan *et al.*[21] when considering scans of $\boldsymbol{Q}$ along [00ℓ] for Ho/Y super-

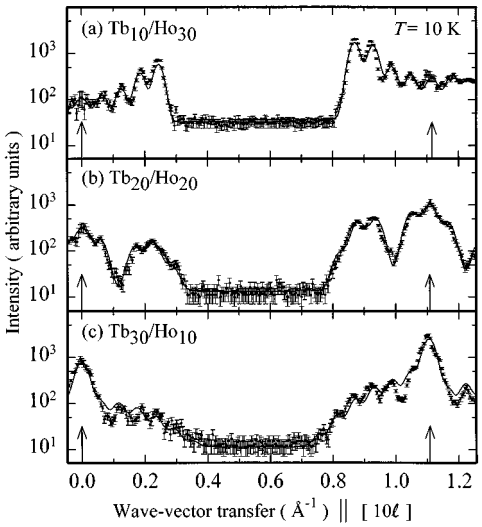

FIG. 4. The points show the magnetic-scattering results at $T=10$ K from scans of wave-vector transfer along $[10\ell]$ using neutrons for the superlattices (a) Tb_{10}/Ho_{30}, (b) Tb_{20}/Ho_{20}, and (c) Tb_{30}/Ho_{10}. The solid lines are fits to the data using the model detailed in Sec. V which simulates a basal-plane ferromagnetic ordering of Tb moments within Tb blocks, and a basal-plane helical ordering of Ho moments. The arrows indicate the positions of the main peaks in the nuclear-scattering measured at $T=290$ K. The equivalence to within a few percent of the scale factors required for fits of the model to data from scans along $[00\ell]$ and $[10\ell]$ indicates that within error, the Tb and Ho moments are confined to the basal plane.

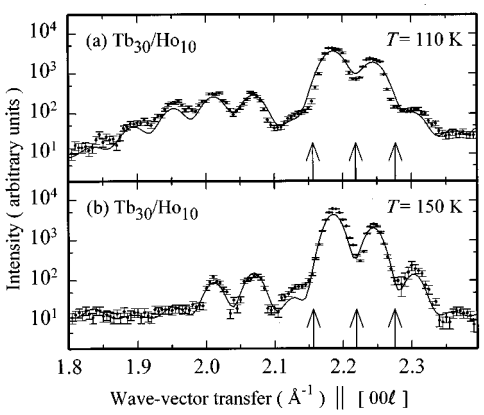

FIG. 5. The points show the magnetic-scattering results for Tb_{30}/Ho_{10} from scans of $\boldsymbol{Q}$ along $[00\ell]$. The arrows indicate the positions of the main peaks in the fits of the model described in Sec. IV to the nuclear scattering at $T=290$ K from the Tb/Ho layers. The solid lines are fits to the data using the model detailed in Sec. V. (a) The measurements were taken at $T=110$ K, and the model used simulates a basal-plane ferromagnetic ordering of Tb moments within Tb blocks, and a basal-plane helical ordering of Ho moments. (b) The measurements were taken at $T=150$ K [i.e., $T>T_N(\mathrm{Ho})$], and the model used simulates a basal-plane ferromagnetic ordering of Tb moments within Tb blocks, and a phase advance over the nonmagnetic Ho layers.

lattices, Φ (modulo 2π) can be calculated using the offset in the position Q_{MAG} of the magnetic peaks, from the position Q_{NUC} of the (002) nuclear peaks, since

$$Q_{\mathrm{NUC}}-Q_{\mathrm{MAG}}=\Phi/L, \tag{2}$$

where L is the bilayer length. For Tb/Ho $\Phi\approx n_{\mathrm{Tb}}\phi_{\mathrm{Tb}}+n_{\mathrm{Ho}}\phi_{\mathrm{Ho}}$, and for a ferromagnetic ordering of Tb moments within blocks ($\phi_{\mathrm{Tb}}=0$),

$$\phi_{\mathrm{Ho}}=\Phi(\mathrm{modulo}\,2\pi)/n_{\mathrm{Ho}}. \tag{3}$$

Therefore, the results from scans of $\boldsymbol{Q}$ in the $[00\ell]$ direction were fitted to a series of Gaussians with, for a given temperature, equal widths and equal separations. L was calculated from the peak separations ($2\pi/L$), values for n_{Ho} were obtained from the fits to the nuclear scattering using x rays and neutrons, and Q_{NUC} was taken from the position of the main (002) Tb/Ho peak at $T=290$ K. The filled circles in Fig. 2 show the temperature dependence of Φ. The initial values for ϕ_{Ho} were then obtained using Eq. (3). The open circles in Fig. 2(c) are calculated values of Φ for Tb_{30}/Ho_{10} above $T\approx200$ K, and will be discussed later. In fitting the models to the data, it was found that overall the best fits (lowest χ^2) were obtained with n_{Tb} and n_{Ho}; and ϕ_{Ho} equal within error to the initial values chosen to within ±0.5 planes and $\pm1°$, respectively. Therefore, the final fits were made with these parameters held at these values.

The model was first fitted to the magnetic scattering from measurements taken at $T=10$ to 130 K. Good fits were obtained, as shown for $T=10$ K by the solid lines in Figs. 3 and 4, when $\boldsymbol{Q}$ is scanned along the directions $[00\ell]$ and $[10\ell]$, respectively. The former scans are sensitive only to the basal-plane ordering of moments, while the latter additionally give information on the moment components along the c axis. The overall scale factors required to fit the models to the data from these two directions differed by less than 5% at all temperatures measured, indicating that the Tb and Ho moments are predominately confined to the basal plane. Figure 5(a) shows the fits to the subtraction results for Tb_{30}/Ho_{10} at $T=110$ K when $\boldsymbol{Q}$ is scanned in the direction $[00\ell]$. Relative to $T=10$ K, the modeling reveals that the shift of the scattering profile to lower $\boldsymbol{Q}$ values largely reflects an increase in ϕ_{Ho}, with the decrease in intensity in the region $(002-q)$ due to the diminishing magnitude of the ordered Ho moments. The contribution to the magnetic scattering from ordered Ho moments falls to zero as the temperature is increased to $T_N(\mathrm{Ho})\approx130$ K.

Above $T\approx130$ K, the model was adapted to simulate the scattering from a basal-plane ferromagnetic ordering of Tb moments within Tb blocks, and a phase advance over the nonmagnetic Ho layers. Good fits were obtained for all samples for temperatures between $T\approx130$ and 200 K. An illustration is given by Fig. 5(b) for Tb_{30}/Ho_{10} at $T=150$ K when $\boldsymbol{Q}$ is scanned along $[00\ell]$. This model also successfully accounts for the results obtained from the samples Tb_{10}/Ho_{30} and Tb_{20}/Ho_{20} as the temperature is raised above $T\approx200$ K, with the intensity of the scattering reducing steadily to zero as the temperature is increased to $T_C(\mathrm{Tb})\approx230$ K.

However, the model cannot describe the results from Tb_{30}/Ho_{10} for measurements made at temperatures above $T\approx200$ K. For this Tb-rich sample additional scattering is observed, for example in the regions $(002\pm q)$ when $\boldsymbol{Q}$ is scanned along $[00\ell]$. The magnitude of the wave vector q is

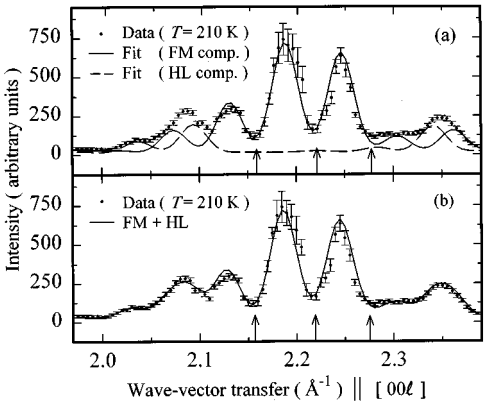

FIG. 6. The points show the magnetic-scattering results at $T=210$ K for Tb_{30}/Ho_{10} when $\boldsymbol{Q}$ is scanned along [00ℓ]. The arrows indicate the positions of the main peaks in the fits of the model described in Sec. IV to the nuclear scattering at $T=290$ K from the Tb/Ho layers. (a) The solid line shows a fit to the data using a model where there is a phase advance across nonmagnetic Ho layers, and a fraction of the Tb moments are ferromagnetically aligned in the basal plane within Tb blocks (FM comp.). The broken line assumes the same ordering of Ho moments as the solid line, but simulates the scattering that would be observed if the remaining fraction of Tb moments were helically aligned in the basal-plane (HEL comp.) (b) The solid line shows the fit to the data from the sum of the two contributions to the scattering shown in (a).

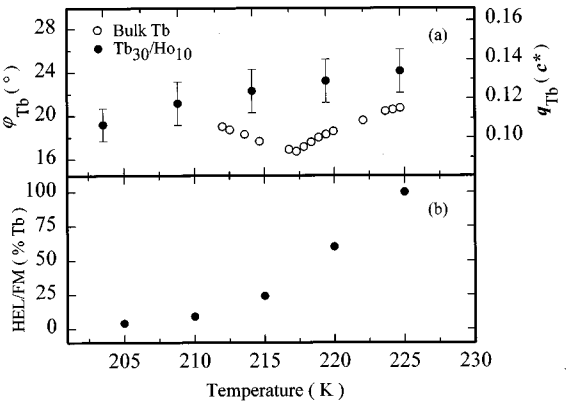

FIG. 7. (a) The turn angle per plane in the Tb blocks $\phi_{Tb}(q_{Tb})$, for the superlattice Tb_{30}/Ho_{10} compared to that of bulk Tb. (b) The temperature dependence of the percentage of Tb moments that in the basal-plane are helically (HEL), as opposed to ferromagnetically (FM) ordered. An extrapolation of these data points to zero was used to deduce the onset of helical ordering in the Tb blocks.

close to that observed for bulk Tb (Ref. 12) when the moments order in a basal-plane spiral between $T\approx216$ and 226 K. To fit the results obtained from measurements of this sample above $T\approx200$ K, further adaptations to the model were required. The total intensity was considered to be the sum of the intensities resulting from the following two structures, with a variable introduced to describe the ratio of the two contributions: a commensurate basal-plane ferromagnetic ordering of Tb moments together with nonmagnetic Ho layers, and an incommensurate ordering of Tb moments in a basal-plane spiral together with nonmagnetic Ho layers. The values for ϕ_{Ho} were allowed to vary independently for the two contributions, but it was found that the optimum fits were achieved with the same ϕ_{Ho} for both contributions. The values for the interface width σ were also allowed to vary independently, and in contrast gave different results for the two scattering contributions. Figure 6 illustrates the construction of the overall profile from these two contributions. The fitted values for ϕ_{Tb} versus temperature are shown in Fig. 7(a) together with those of bulk Tb. The temperature variation of the ratio of the two types of ordering is shown in Fig. 7(b) and it can be seen that between $T\approx200$ and 220 K, there is a mixture of basal-plane helically and ferromagnetically ordered Tb moments, while above $T\approx220$ K there is only a basal-plane helical ordering of Tb moments. No magnetic scattering is observed above $T_N(Tb)\approx230$ K.

Figure 8 illustrates the temperature dependence of ϕ_{Ho} for the Tb/Ho superlattices compared to that of bulk Ho. Using the values of ϕ_{Ho} and ϕ_{Tb}, the values of Φ (modulo 2π) for Tb_{30}/Ho_{10} could be calculated for measurements made above $T\approx200$ K. The results are shown by the open circles in Fig. 2(c).

The coherence lengths ξ of the magnetic structures formed at each temperature could be calculated using Eq. (1) and the widths obtained from the fits (after allowing for instrumental resolution). Figure 9 shows the variation of ξ with temperature for all three samples.

The results from the fits of the models to measurements for which $\boldsymbol{Q}$ was scanned along [00ℓ] were further used to give a more accurate estimation of the limits of the temperature ranges over which the different types of magnetic ordering exist. Values for $T_N(Ho)$ were obtained from the temperature dependence of the fitted magnitude of the ordered Ho moments. The onset of helical ordering of the Tb moments in sample Tb_{30}/Ho_{10} was deduced from Fig. 7(b). Finally, values of $T_C(Tb)$ for Tb_{10}/Ho_{30} and Tb_{20}/Ho_{20}; and the value of $T_N(Tb)$ for Tb_{30}/Ho_{10} were calculated from the temperature variation of the integrated intensity of the total magnetic scattering observed above $T_N(Ho)$. The results from all these calculations are listed in Table II, together with a summary of the magnetic structures that are formed.

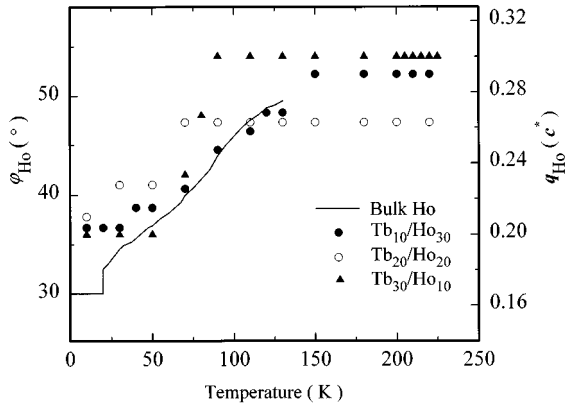

FIG. 8. The turn angle per plane in the Ho blocks, $\phi_{Ho}(q_{Ho})$, for the Tb/Ho superlattices, compared to that of bulk Ho.

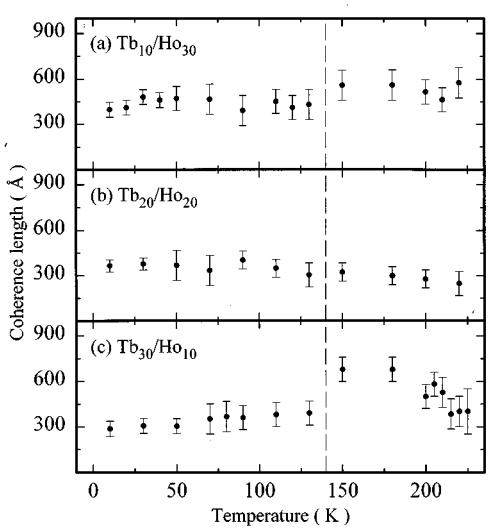

FIG. 9. The temperature dependence of the coherence lengths of the magnetic structures formed in the superlattices (a) Tb_{10}/Ho_{30}, (b) Tb_{20}/Ho_{20}, and (c) Tb_{30}/Ho_{10}. The broken line separates measurements taken at temperatures above and below T_N(Ho).

VI. DISCUSSION

For all temperatures measured, the fits of the models to the results from scans of $\boldsymbol{Q}$ along [00ℓ] and [10ℓ] revealed that the Tb and Ho moments are essentially confined to the basal plane. In bulk Ho, it is the magnetoelastic and dipolar contributions that make it energetically favorable for the moments to cant out of the basal plane below $T \approx 18$ K.[26] Confinement to the basal plane in the Tb/Ho superlattices therefore reflects a change in the relative influence of these interactions, probably partly due to the clamping of the *a* lattice parameters by the Y-seed and capping layers; or by the juxtaposition with Tb for which there is a stronger anisotropy that confines the moments to the basal plane at all temperatures. A similar confinement of Ho moments to the basal plane has been observed for example, in Dy/Ho (Ref. 9) superlattices.

Figure 2 illustrates the temperature dependence of Φ (modulo 2π) and it can be seen that in general (except for the mixed phase region of Tb_{30}/Ho_{10}), $\Phi \approx n\pi/3$. In particular it is noted that $\Phi = \pi$ (modulo 2π) for Tb_{20}/Ho_{20} and Tb_{30}/Ho_{10} above $T \approx 80$ K; and for Tb_{10}/Ho_{30} above T_N(Ho), so that adjacent Tb blocks (within which Tb moments are ferromagnetically aligned) are antiferromagnetically coupled. Such an antiferromagnetic coupling between adjacent ferromagnetic blocks was observed in Gd/Dy (Ref. 7) superlattices at high temperatures, and also in some samples of Dy/Lu (Ref. 4) and Dy/Er (Ref. 27) for which it was suggested to arise from dipolar interactions. In contrast, studies of Gd/Y (Ref. 28) superlattices showed an oscillation between ferromagnetic and antiferromagnetic alignment of adjacent Gd blocks (within which Gd moments were ferromagnetically aligned) as the Y block thickness was varied. The authors proposed that the coupling between adjacent Gd blocks was dominated by an RKKY interaction, and the behavior was a manifestation of oscillations in the sign of the exchange function $\boldsymbol{J}_{\text{Gd-Y}}(\boldsymbol{r})$ with Y block thickness, with a period that depended upon the position of the peak $\chi(\boldsymbol{q})$ for Y. For the Ho thicknesses of the three Tb/Ho superlattices, an RKKY interaction would not be expected to result in the observed antiferromagnetic alignment for *all* samples above T_N(Ho). For Tb/Ho it is probable that at least above T_N(Ho), when the Tb moments remain ferromagnetically ordered dipolar interactions are the dominant influence in determining the magnetic structures. At low temperatures and particularly for the two most Tb-rich samples, the result that $\Phi \approx n\pi/3$ may be related to the basal-plane anisotropy of bulk Tb (Ref. 26) which favors such an alignment of Tb moments along easy axes in the basal plane. This suggestion of the influence of the basal-plane anisotropy in Tb may be supported by comparison with Gd-based superlattices, for which the anisotropy parameters of Gd are several orders of magnitude smaller than those of Tb.[26] For example in Gd/Dy (Ref. 7) superlattices, Φ was in general not equal to $n\pi/3$ at these temperatures, and the details of the magnetic ordering were largely determined by the changes in the Dy turn angle.

The variation of ϕ_{Ho} with temperature is shown in Fig. 8. While restricted by the general condition that $\Phi \approx n\pi/3$ and in particular $\Phi = \pi$ (modulo 2π) at high temperatures, ϕ_{Ho} still qualitatively resembles that of bulk Ho. For a given temperature, ϕ_{Ho} is slightly higher than in the bulk with the difference increasing with the proportion of Tb in the sample. This observation is in accord with previous results[21] that have shown a rise in ϕ_{Ho} when Ho is combined with an element of higher *a* lattice parameter. In more detail, Fig. 8 suggests that below $T \approx 50$ K ϕ_{Ho} locks in within error to either 36° or 40°. Expressed in terms of wave vectors, these values correspond to the commensurable structures $\boldsymbol{q} = (1/5)\boldsymbol{c}^*$ and $\boldsymbol{q} = (2/9)\boldsymbol{c}^*$, respectively. The locking in of ϕ_{Ho} to commensurable values at temperatures below $T \approx 30$

TABLE II. The magnetic properties of the Tb/Ho superlattices deduced from neutron measurements between $T = 10$ and 290 K. The ordering of the Tb and Ho moments was determined by fitting magnetic-structure models based on that developed by Jehan *et al.* (Ref. 21) to the magnetic scattering results from scans of $\boldsymbol{Q}$ along [00ℓ] and [10ℓ]. The methods adopted for calculating T_N(Ho), T_C(Tb), T_N(Tb) and the onset of helical ordering of Tb moments in Tb_{30}/Ho_{10} are described in Sec. V.

Nominal $n_{\text{Tb}}/n_{\text{Ho}}$	Tb FM order Ho HEL order $[T < T_N(\text{Ho})]$ K	Tb FM order Ho no order $[T_N(\text{Ho}) - T]$ K	Tb FM+HEL order Ho no order $[T - T_C(\text{Tb})]$ K	Tb HEL order Ho no order $[T_C(\text{Tb}) - T_N(\text{Tb})]$ K
10/30	$T < 134 \pm 2$	$134 \pm 2 - 231 \pm 2$		
20/20	$T < 132 \pm 1$	$132 \pm 1 - 231 \pm 2$		
30/10	$T < 133 \pm 1$	$133 \pm 1 - 220 \pm 4$	$203 \pm 5 - 220 \pm 4$	$220 \pm 4 - 235 \pm 4$

K has been found in most previously studied Ho-based superlattices.[8,6]

Above $T \approx 200$ K, perhaps the most notable result for Tb_{10}/Ho_{30} and Tb_{20}/Ho_{20} is the suppression of the helical ordering of Tb moments that occurs between $T \approx 216$ and 226 K in bulk Tb.[12] The narrowness of this temperature region reflects the very small difference in the energy of the helical and ferromagnetic phases. Inclusion in a superlattice with a substantial fraction of Ho disrupts this balance, and although the Tb moments still order magnetically at a similar temperature to that in the bulk, they immediately adopt a basal-plane ferromagnetic structure. This may be caused by the basal-plane strain in the superlattices, since bulk Ho has a smaller a lattice parameter than bulk Tb, and a basal-plane contraction has been found to enhance the transition temperature to a ferromagnetic phase, for example in Dy/Lu (Ref. 4) superlattices. In contrast, a suppression of the helical Tb phase was also reported for Tb/Y superlattices[18] despite the strain introduced by Y favoring the helical phase, and the broadening of the range of the helical phase detected in Tb:Y alloys.[11]

For the most Tb-rich sample Tb_{30}/Ho_{10}, the Tb moments *do* order in a basal-plane helix at approximately the same temperatures as observed in the bulk.[12] As recorded in Table I, the fits to the nuclear scattering obtained using x rays indicate that at $T = 290$ K this sample has the smallest difference in d spacings for the constituent elements, suggesting it may be the least strained of the three samples, and therefore is likely to exhibit magnetic properties that are qualitatively most similar to those of bulk Tb. However, the details of the helical ordering for the Tb_{30}/Ho_{10} differ from those of bulk Tb. A mixed phase of basal-plane helically and ferromagnetically aligned Tb moments is observed between $T \approx 200$ and 220 K in the superlattice, compared to between $T \approx 212$ and 216 K in bulk Tb.[12] This extension of the mixed phase region in the superlattice may be due to there being more strain in the region near the substrate, so that the balance of exchange and magnetoelastic energies is not as uniform over the superlattices as in bulk Tb. The ordering in the superlattice also differs from that of bulk Tb in that for a given temperature ϕ_{Tb} is higher than in the bulk,[12] as illustrated in Fig. 7. Studies of alloys of Tb with Ho (Refs. 29 and 30) have found a similar increase of the turn angle associated with helical ordering with for example,[30] a variation between 21.4 and 31.1° for an alloy of 80% Tb with 20% Ho, compared to 16.4 and 20.7° in bulk Tb.[12] This elevation has been explained[5] by assuming that the turn angle is related to the position of the peak in $\chi(\boldsymbol{q})$ for the alloy, which is between that of bulk Tb and Ho. A similar effect may be operative in the Tb/Ho superlattices. A further contrast between the behavior of ϕ_{Tb} for Tb_{30}/Ho_{10} and that of bulk Tb is that while for the superlattice ϕ_{Tb} increases with increasing temperature in the mixed phase region, Dietrich and Als-Nielsen[12] report a decrease which has yet to be fully explained.[12]

Continuing to consider the mixed phase region of Tb_{30}/Ho_{10}, it is interesting to note that the fitted values of the interface parameters for the two separate contributions to the overall scattering are different. For the interface between ferromagnetically aligned Tb moments with the (helical) Ho layers, σ is found to rise from 4 in the pure phase, to 5 or 6 in the mixed phase. However, σ for the interface between helically aligned Tb moments and the Ho layers is found to be 4. The increase in σ for the ferromagnetic/helical interface is perhaps not unreasonable given the lack of uniformity associated with the mixed phase. It is more difficult to explain why the helical/helical interface parameter is not of the same magnitude. It is possible that the helical/helical interface width is inherently smaller, since the structures are better matched electronically. Support for this is given by the work of Simpson *et al.*[31] on Dy/Ho superlattices. Using the same function to model the behavior at the interfaces σ was found to be 2 or 3 for temperatures at which both the Dy and Ho moments were helically ordered in the basal plane. The inequivalence of the values of σ for the two mixed phase contributions in Tb_{30}/Ho_{10} may reflect a difference in the mechanisms involved in the interlayer coupling.

Finally, we discuss the coherence lengths of the magnetic structures that have been identified. As illustrated in Fig. 9, it is found that at all temperatures measured the magnetic ordering is long ranged with coherence lengths extending over approximately three to six bilayers. For Tb/Y (Ref. 18) superlattices it was reported that there was at most only a short-range coherence of the ferromagnetic ordering of Tb moments within Tb blocks, with adjacent Tb blocks antiferromagnetically coupled. This contrasts with the long-range coherence detected for this type of structure for all three Tb/Ho samples. The coherence lengths illustrated in Fig. 9 for Tb/Ho indicate a possible rise in ξ for measurements at temperatures above T_N(Ho), compared to measurements below T_N(Ho) when both the Tb and Ho moments are magnetically ordered. This change in ξ might be related to a change in the relative strengths or the type of mechanisms affecting the interlayer coupling for these two temperature regimes, with the effect particularly enhanced for this the most Tb-rich of the three samples. We consider four factors that may be involved in the interlayer coupling for the Tb/Ho superlattices.

Firstly as discussed above, dipolar interactions may be influential at all temperatures for which the Tb moments remain ferromagnetically aligned. The result that $\Phi = \pi$ (modulo 2π) for all samples at temperatures above T_N(Ho) (except for the mixed phase region of Tb_{30}/Ho_{10}) together with the range of Ho block thicknesses for the three samples, suggests that dipolar interactions are probably dominant at these temperatures. Secondly, coupling based upon an RKKY interaction could be operable at all temperatures. Conventional models based upon this interaction emphasize the role of the peak in $\chi(\boldsymbol{q})$ in determining the possibility of coherent magnetic ordering. Calculations for $\chi(\boldsymbol{q})$ of Tb (Ref. 32) are complicated by spin-disorder scattering but indicate a peak that in comparison to that of Ho (Ref. 26) allows for the possibility of coherent ordering. In the mixed phase region of Tb_{30}/Ho_{10}, Φ is not equal to π and RKKY interactions may be relatively more important since the dipolar interactions are much smaller than when the Tb moments are purely ferromagnetically aligned. As a third possibility, when both the Tb and Ho moments are magnetically ordered nearest-neighbor exchange interactions can give rise to an ordered structure. As outlined in Sec. I these interactions were proposed to be dominant in some Gd/Dy (Ref. 7) superlattices.

As a fourth mechanism, we consider the approach that has recently been put forward to describe cases for which long-range order is achieved by the establishment of a coherent band structure for the whole superlattice.[8,9] These ideas were used to explain for instance, the suppression of the ferromagnetic phase of bulk Dy in Dy/Ho (Ref. 9) superlattices, for which it was suggested that the band structures of Dy and Ho are so similar that they adopt a coherent band structure at the expense of the Dy remaining helical. In order to achieve long-range coherence via the establishment of a coherent band structure in this way, it is proposed that there must be a matching at the interfaces of wave functions associated with the magnetic structures of the superlattice constituents. The existence of both ferromagnetic and helical ordering leads to different wave functions at the interfaces, and so the ferromagnetic transition is suppressed. Given this interpretation, the energy gain of a coherent band structure for Tb/Ho superlattices is not sufficient to overcome the energy required for say, Tb to be forced to remain in the helical phase. This model suggests then, that the coherence that is observed in Tb/Ho superlattices for ferromagnetic/helical structures cannot be attributed to the establishment of an overall coherent band structure.

In order to study further the magnetic properties of superlattice combinations with the potential for ferromagnetic and helical ordering, experiments on Gd/Ho (Ref. 33) superlattices are in progress, and will be reported elsewhere.

In summary, we have investigated the magnetic properties of Tb/Ho superlattices grown by MBE. Four different magnetic ordering regimes were identified, with in all cases the Tb and Ho moments confined to the basal plane: ferromagnetically ordered Tb coherent with helically ordered Ho; ferromagnetically ordered Tb coherent with nonmagnetic Ho; a mixed phase of ferromagnetically and helically ordered Tb together with nonmagnetic Ho; and finally helically ordered Tb together with nonmagnetic Ho. All these structures exhibit long-range ordering, with coherence lengths ranging from three to six bilayers. In discussing the possible mechanisms for interlayer coupling, it is suggested that in addition to conventional RKKY interactions, it may be necessary to consider the influence of nearest-neighbor exchange interactions when the Tb and Ho moments are ordered, and dipolar interactions when there is a ferromagnetic ordering of Tb moments.

ACKNOWLEDGMENTS

We would like to acknowledge the support of the technical staff at Risø and advice from J.A. Simpson. The growth facility and x-ray experiments in Oxford were funded by the EPSRC; and the neutron experiments in Risø by the EU. C.B.-J. is grateful for financial support from the EPSRC.

[1] C.F. Majkrzak, J.W. Cable, J. Kwo, M. Hong, D.B. McWhan, Y. Yafet, J.V. Waszczak, and C. Vettier, Phys. Rev. Lett. **56**, 2700 (1986).

[2] M.B. Salamon, S. Sinha, J.J. Rhyne, J.E. Cunningham, R.W. Erwin, J. Borchers, and C.P. Flynn, Phys. Rev. Lett. **56**, 259 (1986).

[3] Y. Yafet, J. Appl. Phys. **61**, 4058 (1987).

[4] R.S. Beach, J.A. Borchers, R.W. Erwin, M.B. Salamon, B. Everitt, K. Pettit, J.J. Rhyne, and C.P. Flynn, Phys. Rev. Lett. **70**, 3502 (1993).

[5] P.P. Swaddling, R.A. Cowley, R.C.C. Ward, M.R. Wells, and D.F. McMorrow, Phys. Rev. B **53**, 6488 (1996).

[6] C. Bryn-Jacobsen, R.A. Cowley, D.F. McMorrow, J.P. Goff, R.C.C. Ward, and M.R. Wells, Phys. Rev. B **55**, 317 (1997).

[7] C.F. Majkrzak, D. Gibbs, P. Böni, A.I. Goldman, J. Kwo, M. Hong, T.C. Hsieh, R.M. Fleming, D.B. McWhan, Y. Yafet, J.W. Cable, J. Bohr, H. Grimm, and C.L. Chien, J. Appl. Phys. **63**, 3447 (1988).

[8] J.A. Simpson, R.A. Cowley, D.A. Jehan, R.C.C. Ward, M.R. Wells, D.F. McMorrow, K.N. Clausen, T.R. Thurston, and D. Gibbs, Z. Phys. B **101**, 35 (1996).

[9] J.A. Simpson, R.A. Cowley, D.F. McMorrow, R.C.C. Ward, M.R. Wells, C.J. Carlile, and M.A. Adams, J. Phys. Condens. Matter **8**, L187 (1996).

[10] C.F. Majkrzak, J. Kwo, M. Hong, Y. Yafet, D. Gibbs, C.L. Chien, and J. Bohr, Adv. Phys. **40**, 99 (1991).

[11] W.C. Koehler, H.R. Child, E.O. Wollan, and J.W. Cable, J. Appl. Phys. **34**, 1335 (1963).

[12] D.W. Dietrich and J. Als-Nielsen, Phys. Rev. **162**, 315 (1967).

[13] P.M. Gehring, L. Rebelsky, D. Gibbs, and G. Shirane, Phys. Rev. B **45**, 243 (1992).

[14] W.C. Koehler, J.W. Cable, M.K. Wilkinson, and F.O. Wollan, Phys. Rev. **151**, 414 (1966).

[15] D. Gibbs, D.E. Moncton, K.L. D'Amico, J. Bohr, and B.H. Grier, Phys. Rev. Lett. **55**, 234 (1985).

[16] R.A. Cowley and S. Bates, J. Phys. C. **21**, 4113 (1988).

[17] J.A. Simpson, D.F. McMorrow, R.A. Cowley, and D.A. Jehan, Phys. Rev. B **51**, 16 073 (1995).

[18] C. Dufour, K. Dumesnil, M. Vergnat, P. Mangin, G. Marchal, and M. Hennion, J. Magn. Magn. Mater. **140**, 771 (1995).

[19] M.K. Wilkinson, W.C. Koehler, E.O. Wollan, and J.W. Cable, J. Appl. Phys. **32**, 48S (1961).

[20] R.E. Camley, J. Kwo, M. Hong, and C.L. Chien, Phys. Rev. Lett. **64**, 2703 (1990).

[21] D.A. Jehan, D.F. McMorrow, R.A. Cowley, R.C.C. Ward, M.R. Wells, N. Hagmann, and K.N. Clausen, Phys. Rev. B **48**, 5594 (1993).

[22] J. Kwo, E.M. Gyorgy, D.B. McWhan, M. Hong, F.J. DiSalvo, C. Vettier, and J.E. Bower, Phys. Rev. Lett. **55**, 1402 (1985).

[23] G. L. Squires, *Introduction to the Theory of Thermal Neutron Scattering* (Cambridge University Press, Cambridge, 1978).

[24] J.P. Goff, C. Bryn-Jacobsen, D.F. McMorrow, R.C.C. Ward, and M.R. Wells (unpublished).

[25] J.A. Simpson, D.F. McMorrow, R.A. Cowley, M.R. Wells, and R.C.C. Ward, J. Phys. Condens. Matter **7**, L417 (1995).

[26] J. Jensen and A.R. Mackintosh, *Rare Earth Magnetism - Structures and Excitations* (Oxford Science, New York, 1991), Vol. 1.

[27] K. Dumesnil, C. Dufour, Ph. Magin, G. Marchal, M. Henion, H. Kaiser, and J.J. Rhyne, J. Magn. Magn. Mater. **140**, 775 (1995).

[28] J. Kwo, M. Hong, F.J. DiSalvo, J.V. Waszczak, and C.F. Ma-

jkrzak, Phys. Rev. B **35**, 7295 (1987).
[29] F.H. Spedding, Y. Ito, R.G. Jordan, and J. Croat, J. Chem. Phys. **54**, 1995 (1971).
[30] B. Lebech, Solid State Commun. **6**, 761 (1968).
[31] J.A. Simpson, R.A. Cowley, and D.F. McMorrow (private communication).
[32] S.H. Lui, R.P. Gupta, and S.K. Sinha, Phys. Rev. B **4**, 1100 (1971).
[33] C. Bryn-Jacobsen, R.A. Cowley, D.F. McMorrow, R.C.C. Ward, and M.R. Wells (unpublished).